J Mater Sci (2009) 44:861–868
DOI 10.1007/s10853-008-3185-x

Rutile thin film responsive to visible light and with high UV light sensitivity

Hiroki Nagai · Sohei Aoyama · Hiroki Hara · Chihiro Mochizuki · Ichiro Takano · Norio Baba · Mitsunobu Sato

Received: 22 September 2008 / Accepted: 11 December 2008 / Published online: 31 December 2008

Abstract A transparent rutile thin film 100 nm thick was fabricated on a quartz glass substrate; it was responsive to visible light and had a higher sensitivity to UV light than an anatase thin film formed by sol–gel method under identical conditions. The crystal structure was determined by observations using X-ray diffraction, Raman spectra, and a transmission electron microscope. The oxygen/titanium ratio of the rutile thin films was 1.78 according to the XPS peaks. The photoreactivity and photoinduced hydrophilicity of the rutile thin films was examined by measuring the pseudo first-order rate for the decoloration of methylene blue in an aqueous solution and the water contact angle, respectively. The high photoreactivity and photosensitivity of the O-deficient rutile thin film, whose optical band edge and refractive index were 3.10 eV and 2.2, respectively, were due to electron traps and assisted by O-defects within the rutile particles.

H. Nagai · S. Aoyama · H. Hara · C. Mochizuki · M. Sato (✉)
Coordination Engineering Laboratory, Faculty of Engineering, Kogakuin University, 2665-1 Nakano, Hachioji City, Tokyo 192-0015, Japan
e-mail: lccsato@cc.kogakuin.ac.jp; ft10302@ns.kogakuin.ac.jp

H. Nagai
e-mail: bd06002@ns.kogakuin.ac.jp

I. Takano
Department of Electrical Engineering, Faculty of Engineering, Kogakuin University, 2665-1 Nakano, Hachioji City, Tokyo 192-0015, Japan

N. Baba
Department of Information Science, Faculty of Informatics, Kogakuin University, 2665-1 Nakano, Hachioji City, Tokyo 192-0015, Japan

Introduction

Titania (TiO_2) has received considerable attention as a naturally abundant photosensitive material; rutile and anatase, both titania polymorphs, are industrially available. Rutile is the most stable crystal form of titania [1–4]. So far, anatase has been found to be more photosensitive than rutile. Since Nishimoto et al. showed that anatase is more sensitive to UV light than rutile in a photoreaction, rutile was believed to be inferior to anatase in terms of photoreactivity [5, 6]. Anatase is important for photocatalysis in pollutant degradation and in the development of photofunctional materials, such as films with hydrophilic surfaces, under UV light irradiation. The poor photoreactivity and photosensitivity of rutile are generally believed to be due to its crystal structure [6, 7], so rutile is primarily known as a useful pigment for white paint due to its chemical stability. Rutile more photosensitive than anatase has not yet been discovered; however, in 1972 Fujishima and Honda observed that water molecules photodecomposed on rutile being irradiated by UV light when a certain electric potential was applied to a Pt counter electrode [8].

Anatase, which responds only to UV light, has recently become the focus of research studies attempting to get it to respond to visible light in order to utilize solar and interior light efficiently. Layer-structured anatase thin films, when fabricated by heat treating molecular precursor films under an argon gas flow, were found to respond to visible light with enhanced UV sensitivity by the authors of this study in a previous article [9]. Recently, further details were provided revealing that the uniquely enhanced UV sensitivity of these anatase thin films was caused by oxygen deficiencies embedded within the anatase [10].

Because the band edge of a rutile single crystal is 3.0 eV, rutile has the potential to respond to visible light

[11]. Based upon this knowledge and building upon the results from the previous experiments on anatase responsiveness to visible light, this article details an attempt toward the direct fabrication of O-deficient rutile thin films with high photoreactivity by using a molecular precursor method. The first visible light-responsive thin film created from O-deficient rutile is discussed here; it works without applying any electric potential because of its unprecedented high photosensitivity under UV light irradiation. The findings of this study should facilitate widespread practical use of rutile in light-related applications.

Experimental

Materials

Ethylenediamine-*N,N,N′,N′*-tetraacetic acid (EDTA), methylene blue (MB), and titanium tetraisopropoxide ($Ti(O^iPr)_4$) were purchased from Kanto Chemical Co., Inc. Dibutylamine and 30% H_2O_2 were purchased from Wako Pure Chemical Industries, Ltd., and from Santoku Chemical Industries Co. Ltd., respectively. Methanol and 60% HNO_3 were purchased from Taisei Chemical Co. Ltd. Ethanol was purchased from Ueno Chemical Industries, Ltd. These solvents were dried in 4A molecular sieves before use. Other materials were used without further purification. Quartz glass was purchased from Akishima Glass. The glass substrates with dimensions of $20 \times 20 \times 1.1$ mm^3 were washed in 2-propanol for 15 min with sonicated stirring and then dried in a drying oven at 70 °C.

Preparation of the precursor solution S_{MP} involving the Ti^{4+} complex of EDTA

The precursor solution containing Ti^{4+} complex of EDTA was obtained by a method modified from the one previously reported by the authors [9, 10, 12]. Dibutylamine, 3.58 g (27.7 mmol) and EDTA, 3.56 g (12.2 mmol) were added to a mixture of 10 g each of ethanol and methanol, respectively. The solution was refluxed for 2 h with stirring and then cooled to room temperature. After adding 3.47 g (12.2 mmol) of $Ti(O^iPr)_4$, the solution was refluxed for 4.5 h. After cooling the reacted solution to room temperature, 1.56 g (13.8 mmol) of 30% H_2O_2 was carefully added. The solution was then refluxed for 0.5 h. The concentration of titanium was 0.4 mmol g^{-1}.

Preparation of the sol–gel solution S_{SG}

A conventional sol–gel solution was prepared by reacting 4.31 g (15.2 mmol) of $Ti(O^iPr)_4$ with 1.10 g (10.5 mmol) of 60% nitric acid and 0.84 g (46.7 mmol) of water in 25 g of ethanol [13, 14]. The concentration of titanium was 0.5 mmol g^{-1}.

Coating, heat-treating procedures, and film thickness

The thin films were formed by heat-treating the precursor films (15×15 mm^2) spin-coated onto a quartz glass substrate; the solutions S_{MP} and S_{SG} were applied with an argon gas flow. A spin-coating method to form the titania precursor films were formed with a spin-coating method employed with a double step each time: first at 500 rpm for 5 s, then at 2,000 rpm for 30 s. Transparent precursor films formed by spin-coating the solutions and pre-heating in a drying oven at 70 °C for 10 min were heat-treated at 700 °C for 30 min in a furnace made from a quartz tube (φ 40 mm) with an argon gas flow rate of 0.1 L min^{-1}. When S_{MP} was used, a transparent rutile thin film **R** formed; when S_{SG} was used, a transparent anatase thin film **A** formed. The film thickness, measured using the stylus profilometer DEKTAK3, was 100 nm in both cases.

In order to prepare the samples for transmission electron microscope observation, ultra-thin films with film thicknesses of 10 nm were prepared using 1/10-diluted solutions of S_{MP} and S_{SG} and under the same conditions except for the solution concentration and the substrate. NaCl single crystals were employed for the substrate instead. The ultra-thin films were fabricated and then recovered by dissolving the NaCl substrate with water.

Structure and chemical identity of thin films

The X-ray diffraction (XRD) pattern of each film was measured with an X-ray diffractometer (MXP-18 AHF22, Bruker AXS), with Cu–$K\alpha$ rays generated at 45 kV and 300 mA. Parallel beam optics with an incident angle of 3.0° was employed. Cell parameters were refined by the least square method.

The structure and lattice image of each film were observed with a transmission electron microscope (TEM H8100, Hitachi) at an accelerating voltage of 200 kV and the ultra-thin films applied on a Cu grid.

A Phi Quantum 2000 Scanning ESCA Microprobe (Shimadzu) with a focused monochromatic Al–$K\alpha$ X-ray (1486.6 eV) source was employed in order to evaluate the element states and quantities—Ti, O, N, and C—in the films. Chemical shift data were charge-referenced to the center of the C–C/C–H peak at 284.6 eV. The resolution was 0.2 eV for each measurement. The depth profile was obtained with the same instrument. The stepwise etching was performed by bombarding the Ar^+ ion with 2 kV and 18 μA cm^{-2} for 3 min before measuring each layer. The XPS peaks for all the 15 layers were measured in order to obtain the depth profile.

Surface morphology and mechanical strength

The surface appearance of the thin films coated with gold was observed with a field-emission scanning electron microscope (FE-SEM S-4200, Hitachi) at an accelerating voltage of 5 kV.

The adhering strength of the films to the quartz substrate was examined with a scratch tester (HEIDON-22, Shinto Scientific) using a load of 0.50 kg and a scanning rate of 10.5 N min^{-1}.

Optical properties of thin films

The transmittance and absorption spectra of the thin films were measured in the 200–800 nm range with a double-beam mode; the quartz glass substrate was used as the reference for each measurement. The measurements were performed with a U-2800 spectrophotometer (Hitachi). The optical band edge E_g of the thin films was determined by using the following Tauc expression:

$$\alpha = \frac{A(E - E_g)^{1/2}}{E} \quad (1)$$

where E is the photon energy ($\equiv h\nu$); A is the constant; and α is the absorption coefficient at the wavelength [15].

A MARY-102 (Five Lab) scanning ellipsometer was employed to measure the refractive index of the thin films with a He–Ne laser beam of 632.8 nm and an incidence angle of 70.8°. The refractive index was measured three times at eight different points on the thin films and averaged to determine the value.

Photoreactivity measurements

The photoreactivity of each film was examined using the decoloration rate of methylene blue (MB) in 10 mL of aqueous solution (0.01 mmol L^{-1}). A black light (FL10BL-B, National), was used for UV light irradiation. The distance of the black light source from the sample surfaces was adjusted in order to maintain a UV light intensity of 1.2 mW cm^{-2} at 365 nm; the intensity was measured with an ultraviolet meter (UVR-400, Iuchi). The visible light intensity on the samples was 0.8 mW cm^{-2} with the fluorescent light (True light, Duro Test) after removing wavelengths shorter than 400 nm by using a cut-off filter; the intensity was measured with an illuminometer (LX-105, Custom). The removal of UV light was confirmed by checking the UV light intensity for a value of 0.0 mW cm^{-2} at 365 nm with the UV meter.

The MB concentration was determined by measuring the absorption spectra of the aqueous solution with the U-2800 spectrophotometer. For the decoloration test, 3 mL of the solution was transferred into a quartz cell of dimensions $1 \times 1 \times 4.5$ cm^3 at 20-min intervals. After spectral measurement, the solution was immediately returned to the vessel and mixed with the aliquot. The mixed solution continued to be used until the test for each film was completed. The temperature of the test solution was maintained at 20 ± 1 °C throughout the measurement.

The pseudo first-order rate for the decoloration reaction of the MB aqueous solutions was obtained three times for each film; the averaged value was assigned to the rate v. In order to examine the effects of both the adsorption and the self-decoloration for MB, the same measurement was performed on the same samples without irradiation as a reference. The v value for each film was calculated as follows. The MB concentration C(t) after irradiation for t min was determined as

$$C(t) = 10 \times \frac{Abs(t)}{Abs(0)} [\mu\text{mol L}^{-1}] \quad (2)$$

where $Abs(0)$ and $Abs(t)$ represent the absorption value at 664 nm for the solution immediately before irradiation and after irradiation for t min, respectively. An approximate line for the function of C(t) versus t was obtained in the range $0 \leq t \leq 80$ min by the least square method. The rate v for each film was estimated as the averaged gradient of the lines:

$$v = \frac{|\sum v_n|}{3} \times 10^3 \quad [\text{nmol L}^{-1}\,\text{min}^{-1}], \quad (3)$$

where v_n indicates each of the individual gradients ($n = 1$, 2, 3) obtained independently.

Photo-induced hydrophilicity measurements

The contact angle for a 1.0-μL water droplet on the thin films was measured with a contact angle meter (FACE, Kyowa Kaimenkagaku). The measurement was performed after irradiation of the samples with visible or UV light in atmospheric air at 26 °C and 40% humidity. The same light sources employed in the decoloration test for the MB solution mentioned above were used. In this experiment, the position of the black light source was adjusted in order to maintain a UV intensity of 4.5 mW cm^{-2} at 365 nm on the samples. The contact angle for the water droplet before the light irradiation on **R** (68°) was almost the same as for **A** (70°) under the same atmospheric conditions.

Results

Crystal structure and chemical identity of the thin films

Figure 1 shows the XRD patterns for **R** and **A**. In **R**, the peaks were found at $2\theta = 27.5$, 36.2, 39.3, 41.4, 44.3, 54.5,

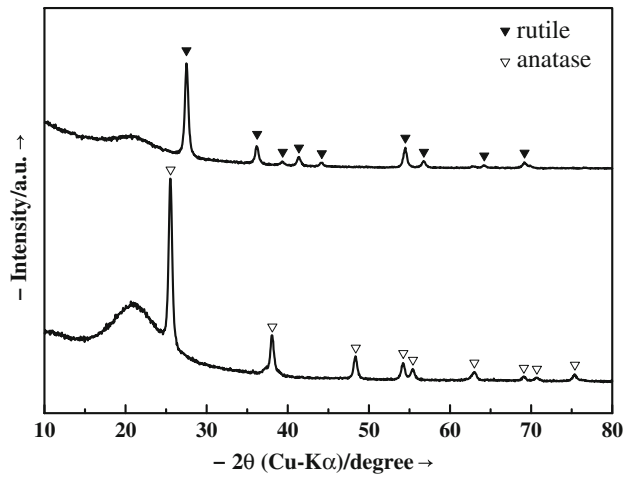

Fig. 1 XRD patterns for **R** (rutile) and **A** (anatase) fabricated by heat treating the corresponding precursor film at 700 °C in an Ar gas flow

56.7, 64.2, and 69.2°, corresponding to the (110), (101), (200), (111), (210), (211), (220), (310), and (301) phases of rutile [16]. In **A**, the peaks were observed at $2\theta = 25.6$, 38.1, 48.4, 54.2, 55.5, 62.9, 69.1, 70.7, and 75.3°, corresponding to the (101), (004), (200), (105), (211), (204), (116), (220), and (215) phases of anatase [17]. The precise cell parameters for the tetragonal lattices were $a = 0.459(1)$ nm and $c = 0.296(1)$ nm for **R**, and $a = 0.377(1)$ nm and $I = 0.953(4)$ nm for **A**. These values correlated well with the corresponding lattices for the rutile and anatase crystals. Thus, the crystal structures of **R** and **A** were demonstrated to be the single phases of rutile and anatase, respectively.

The Raman spectra of **R** and **A** thin films are shown in Fig. 2. The absorption bands at 139, 441, and 609 cm^{-1} correspond to rutile in the spectrum for **R**. The absorption bands at 146, 400, 521, and 641 cm^{-1} correspond to anatase in the spectrum for **A** [18].

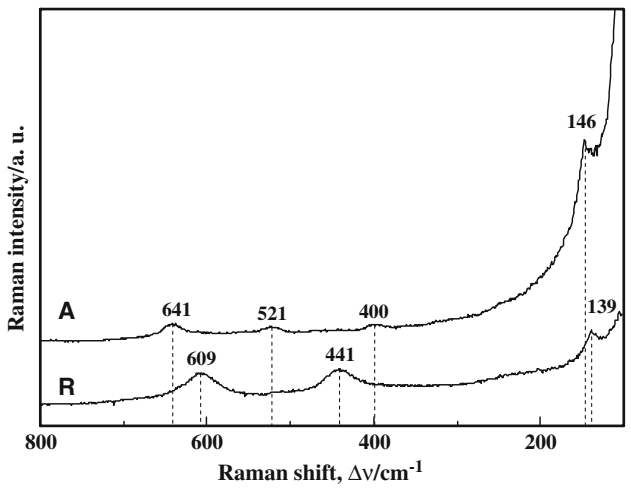

Fig. 2 Raman spectra for **R** and **A** thin films fabricated by heat treating the corresponding precursor film at 700 °C in an Ar gas flow

The transmission electron microscope (TEM) images and electron diffraction patterns for the ultra-thin films corresponding to **R** and **A** are presented in Fig. 3, along with the phase assignment and dimension. The diffraction patterns indicated a typical tetragonal structure for rutile and anatase with the corresponding cell parameters. These results were consistent with those determined by the XRD patterns for **R** and **A**.

The XPS peaks corresponding to O 1s and Ti $2p_{3/2}$ were found at 529.8 eV and 458.8 eV, respectively, for each film; these values are typical for titania [19]. The averaged O/Ti peak area ratio was 1.78 for **R** and 1.93 for **A**. The homogeneity in the vertical direction of the thin films was confirmed by the depth profiles of the XPS peaks, which were measured with an Ar^+ ion etching mode.

Surface morphology and mechanical strength of the thin films

The surface appearance of the thin films is shown in Fig. 4.

The adhering strength of **R** and **A** to the quartz substrate was 1.75 and 0.69 GPa, respectively.

Optical properties of the thin films

The transmittance spectra of the thin films are presented in Fig. 5. The optical band edge for **R**, determined from the corresponding absorption spectrum by assuming a direct-transition semiconductor, was 3.10 eV; it was considerably smaller than for **A** (3.63 eV).

The refractive indices of **R** and **A** were 2.2 and 2.5, respectively.

Photoreactivity of thin films

The photoreactivity of the thin films was evaluated by the decoloration rate of the MB solution, which served as a model for organic pollutants in water [20, 21]. The results measured under visible and UV light irradiation are summarized in Table 1 along with those measured under dark conditions (reference values); they indicate the effects of adsorption on the samples and vessels and self-decoloration of MB under each condition [9, 10]. The v values, where v is the pseudo first-order rate, were found to be larger than when under dark conditions, indicating the degree of photoreaction induced by the light irradiation on the films. Rapid decoloration of the MB solution due to the redox reaction caused by **R** was clearly observed when irradiating the films with only visible light. Moreover, the photoreactivity of **R** was also extremely high under UV light

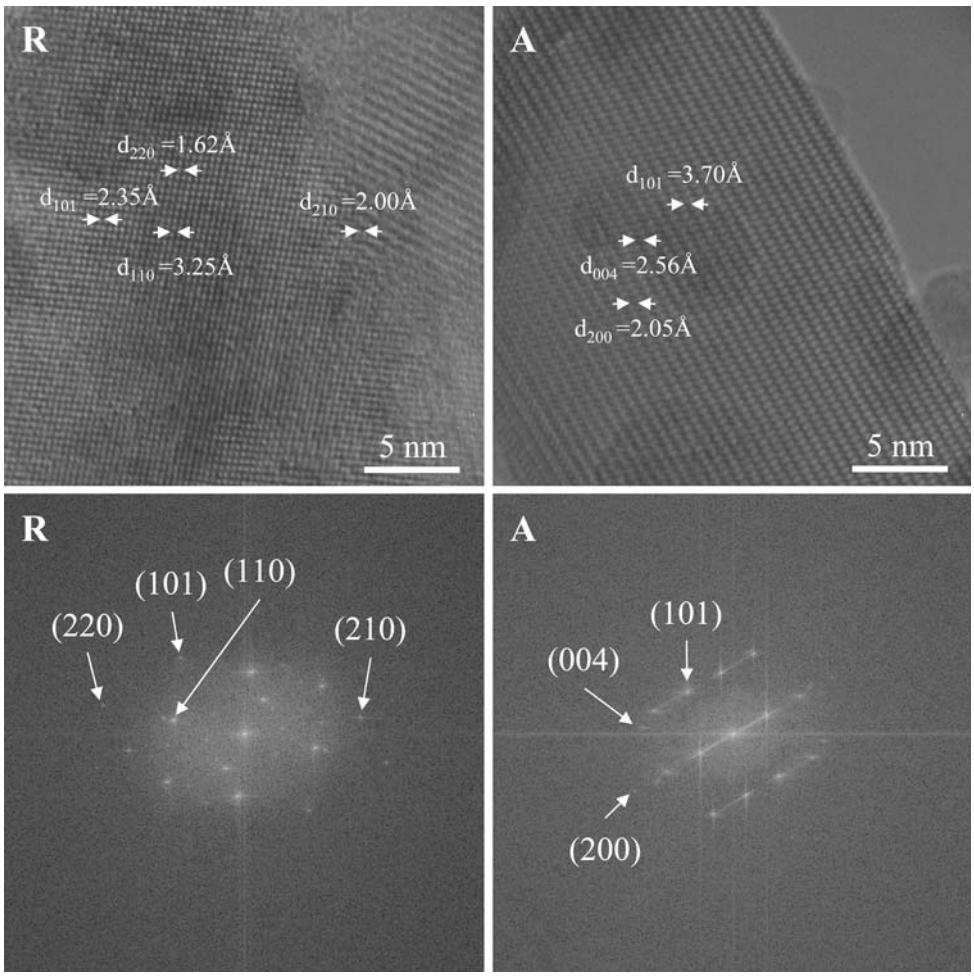

Fig. 3 Structure and lattice image of the ultra-thin films corresponding to **R** and **A**, observed with a transmission electron microscope. The TEM images (above) and the corresponding diffraction patterns (below) of the films are described, respectively. The crystal structure was analyzed using Fourier-transformed patterns

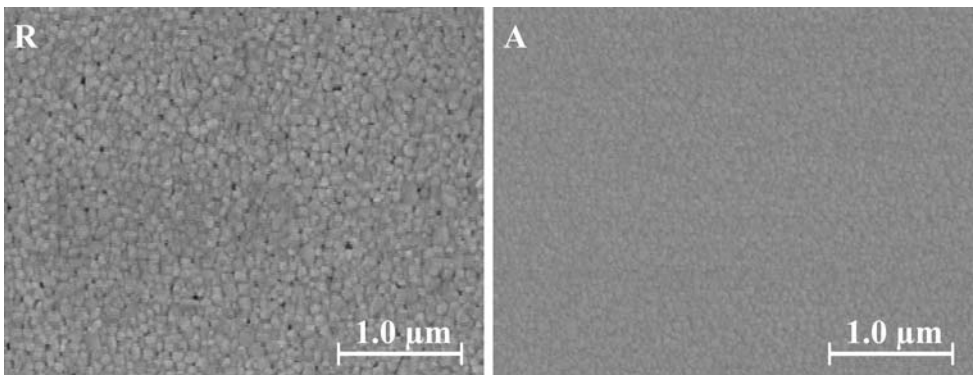

Fig. 4 Surface appearance of **R** and **A** observed by using a field emission scanning electron microscope

irradiation and higher than the photoreactivity of **A**, which is without precedent.

Photoinduced hydrophilicity of thin films

The photosensitivity of **R** and **A** was also examined by measuring the effects of visible and UV light irradiation on the water contact angle for the surfaces of the thin films [22–24]. The results are shown in Fig. 6. The rutile thin-film **R** exhibited visible light-induced hydrophilicity with a fluorescent light even though high-energy light with wavelengths shorter than 400 nm was eliminated. In contrast, visible light alone did not effectively reduce the contact angle on **A** under the same conditions. Furthermore, a rapid decrease in the water contact angle for **R** was observed with weak UV light irradiation. The superhydrophilic property of **R** appeared after only 1 h. When fluorescent light with a UV component was employed, the

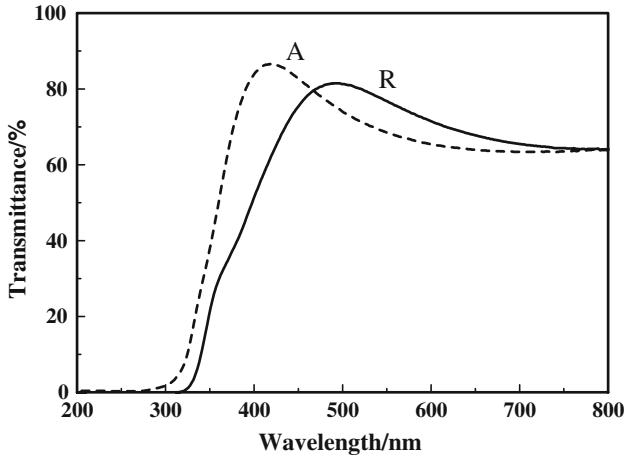

Fig. 5 Transmittance spectra of **R** and **A** for the 100-nm-thick film on a quartz substrate. The solid and broken lines indicate the **R** and **A** thin films, respectively

Table 1 The pseudo first-order kinetic rate v for the decoloration reaction in an aqueous solution containing 0.01 mol L^{-1} of methylene blue under both visible and UV light irradiation and under dark conditions

Notation	v [nmol L^{-1} min^{-1}][a]		
	Under visible light	Under UV light	Under dark conditions
R	13.3 (2)	26.7 (2)	4.2 (1)
A	3.8 (1)	19.3 (1)	3.8 (1)

[a] Estimated standard deviations are presented in parentheses

contact angle on **R** reduced more rapidly and the values reached 38° and 10° after irradiation for 1 and 24 h, respectively.

Discussion

Selective formation of rutile and anatase

Both the rutile and anatase thin films were easily formed selectively at 700 °C despite employing the different coating solutions. Each structure was characterized using XRD, Raman spectra, and TEM observations. The selectivity was due to the fact that the O-vacant sites in the oxide thin films formed at different levels due to the difference in the amount of oxygen between the two precursors; in this study, the oxygen source required to structure titania was available only in the precursor films when these thin films were fabricated. Therefore, crystallization into rutile, which has many O-vacant sites, and the accompanying rapid elimination of organic residues from the **R** precursor film occurred because of the heat treatment.

In contrast, the amount of oxygen available to the Ti^{4+} ions in the titanoxane polymers, though significant, was insufficient to develop stoichiometric TiO_2 from **A**. The oxygen defects in an anatase lattice generally lower the temperature of the phase transformation from anatase to rutile [25]. Thus, selective formation occurred according to differing levels in O-deficiency.

Optical property, surface morphology, and mechanical strength of the thin films

The band edge of **R** was comparable to that for a single crystal of rutile (3.0 eV) [1]. On the other hand, the band edge of **A** was higher than that for a single crystal of anatase, but comparable to anatase thin films with internal stresses caused by a lattice mismatch with the substrate [26]. The well-developed grain boundary in **R** was observed using the FE-SEM and is shown in Fig. 4. When compared to the size of the anatase grains in **A**, the grain sizes of the rutile crystals in **R** were undoubtedly larger. The internal stresses in **R** were relaxed by grain growth, thus reducing the band edge differences between a thin film and a single crystal.

In addition, the refractive index of **R** was lower than for **A**, although in general the index for rutile is higher than anatase [26, 27]. Permittivity is described by the following equation

$$\nabla \cdot \mathbf{E} = \frac{\rho}{\varepsilon_0}, \tag{4}$$

where **E** is the electric field intensity, ρ the charge density, and ε_0 the vacuum permittivity. The fact that the refractive index of **R** was smaller than for **A** suggested that the permittivity of **R** showed an extraordinary decrease due to the low charge density from a high O-deficiency compared to **A**. Therefore, the optical properties of **R** were found to be strongly related to its large O-deficiency.

Furthermore, the adhering strength of **R** to the quartz substrate was more than twice the strength of **A**. The titanium ions of **R** linked covalently to the O atoms belonging to the quartz molecules to form a robust interface between the quartz glass substrate and **R**. The strong adherence to the substrate was assumed to occur because of the many O-defects of **R** compared to **A**.

Inner part electron trap (IPET) effect

From the abovementioned results, the rutile thin film **R** with many O-defects was shown to have high photoreactivity and photoinduced hydrophilicity under both visible and UV light irradiation. Linsebigler et al. proposed that O-vacancies on a titania surface suppress the recombination of photoinduced electron–hole pairs with electron traps and

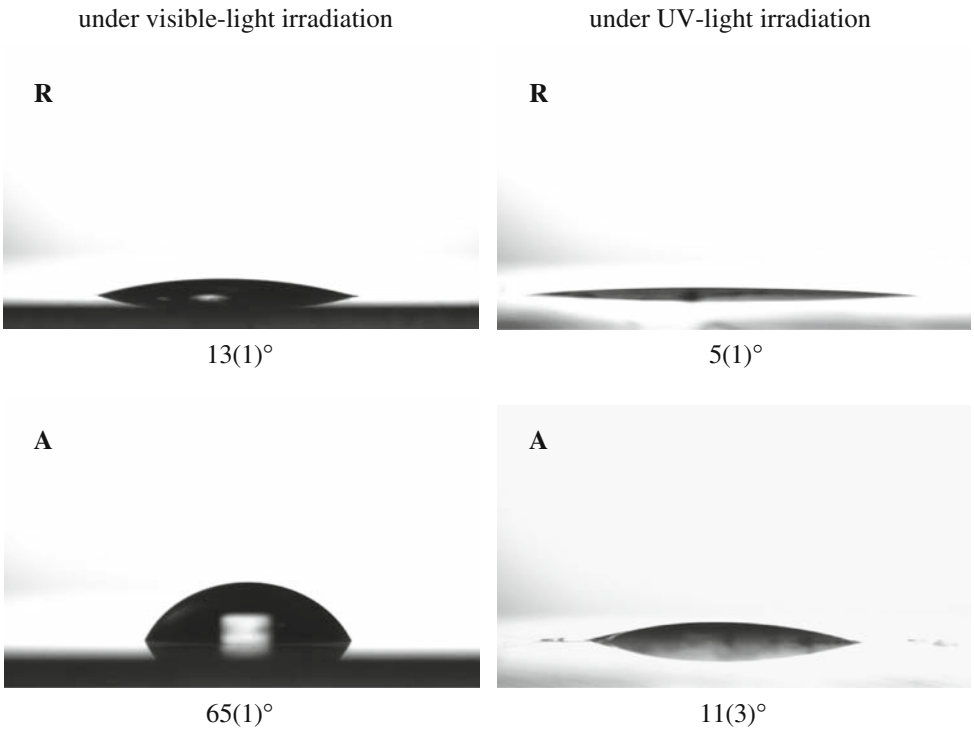

Fig. 6 Comparison of the contact angles for a 1.0-μL water droplet on **R** and **A**. Before measurement, the thin films were exposed either to only visible light (samples on the left), obtained by removing the UV component from the light emitted by a fluorescent lamp, or to UV irradiation (samples on the right), obtained with a black light

thus extend their lifetime [28]. This might lead to the high photoreactivity of O-vacant titania. Previously, several researchers examined the formation of O-vacant sites on a rutile thin-film surface by physical injection of or chemical reduction with hydrogen [29, 30]. However, photoinduced properties for rutile with an O-vacant surface were not observed in those studies, though the modification of its electric properties was shown. This suggests that the photoinduced properties of titania are not effectively assisted by the O-vacant sites on its surface alone. As shown by the XPS examination, many O-defects for **R** were spread throughout much of the rutile thin films formed in this study. Thus, the electron traps caused by O-deficiencies embedded deeply in **R** can be concluded to provide an essential contribution to its effective photoreactivity and photoinduced hydrophilicity under both visible and UV light.

Conclusion

This study presents an alternative method for enabling titania to respond to visible light without using the doping impurities usually employed for visualizing anatase, where the original photoreactivity under UV light irradiation is suppressed by generated impurity levels. This article showed that a certain level of O-deficiency embedded deeply within rutile crystals in the thin film can actualize the intrinsic and potential properties of rutile to respond to visible light. This article proposed an inner part electron trap (IPET) effect by using an O-deficient rutile thin film. In addition, the results led to the recommendation to differentiate rutile and anatase, which are frequently expressed simply as titania, in future study to avoid any confusion while discussing on their respective photoreactivity and photosensitivity. The results from this study should lead to developing applications of rutile thin films to solar energy conversion and the degradation of organics in polluted water and air under solar and interior light, along with the utilization of an anti-foggy surface derived from its hydrophilicity induced by both visible and UV light.

Acknowledgements This study was supported by the High-Tech Research Center Project for Private Universities: Matching Fund Subsidy from MEXT (Ministry of Education, Culture, Sports, Science and Technology) Japan, 2006–2010.

References

1. Weiser HB, Milligan WO (1934) J Phys Chem 38:513
2. Evans RC (1966) An introduction to crystal chemistry, 2nd edn. Cambridge University Press, New York
3. Lindsley DH (1976) Experimental studies of oxide minerals. Mineral Society of America
4. Fahmi A, Minot C, Silvi B, Causá M (1993) Phys Rev B 47:11717
5. Nishimoto S, Ohtani B, Kajiwara H, Kagiya T (1985) J Chem Soc Faraday Trans 1 81:61
6. Follis D, Pelizzetti E, Serpone N (1991) Environ Sci Technol 25:1523
7. Fox MA, Dulay MT (1993) Chem Rev 83:341

8. Fujishima A, Honda K (1972) Nature 238:37
9. Nagai H, Mochizuki C, Hara H, Takano I, Sato M (2008) Sol Energy Mater Solar Cells 92:1136
10. Nagai H, Hasegawa M, Hara H, Mochizuki C, Takano I, Sato M (2008) J Mater Sci 43(21):6902
11. Cronemeyer DC (1952) Phys Rev 87:876
12. Sato M, Hara H, Nishide T, Kuritani H, Sawada Y (1996) J Mater Chem 6:1767
13. Brinker CJ, Scherer GW (1990) Sol–gel science. Academic Press, California
14. Bruce DW, O'Hare D (1992) Inorganic materials. Wiley, Chichester
15. Tanemura S, Miao L, Jin P, Kaneko K, Terai A, Nabatova GN (2003) Appl Surf Sci 212–213:654
16. JCPDS Card 21-1276
17. JCPDS Card 21-1272
18. Ohtsuka T, Guo J, Sato N (1986) J Electrochem Soc 133:2473
19. Moses PR, Wier LM, Lennox JC, Finklea HO, Lenhard JR, Murray RW (1978) Anal Chem 50:576
20. Kwon CH, Shin H, Kim CH, Choi WS, Yoon KH (2004) Mater Chem Phys 86:78
21. Ohno T, Tsubota T, Nishizima K, Miyamoto Z (2004) Chem Lett 33:750
22. Wang R, Hashimoto K, Fujishima A et al (1997) Nature 388:431
23. Watanabe T, Nakajima A, Wang R et al (1999) Thin Solid Films 351:260
24. Machida M, Norimoto K, Watanabe T, Hashimoto K, Fujishima A (1999) J Mater Sci 34:2569. doi:10.1023/A:1004644514653
25. Gennari FC, Pasquevich DM (1998) J Mater Sci 33:1571. doi:10.1023/A:1017515804370
26. Miao L, Jin P, Kaneko K, Terai A, Nabatova-Gabain N, Tanemura S (2003) Appl Surf Sci 212–213:255.
27. Nishide T, Hara H, Sato M (2000) J Mater Sci 35:465. 10.1023/A:1004731804075
28. Linsebigler AL, Lu G, Yates JT (1995) Chem Rev 95:735
29. Hill GJ (1968) J Appl Phys 1:1151
30. Ohmori A, Kyeung CP, Inuzuka M, Arata Y, Inoue K, Iwamoto N (1991) Thin Solid Films 201:1